Article

The Role of APTES as a Primer for Polystyrene Coated AA2024-T3

John Halford IV and Cheng-fu Chen *

Posted Date: 15 December 2023

doi: 10.20944/preprints202312.1156.v1

Keywords: vapor deposition; coating; primer; polystyrene; APTES; silanes; AA2024-T3; corrosion; electrochemical impedance spectroscopy; NaCl

Article

The Role of APTES as a Primer for Polystyrene Coated AA2024-T3

John Halford IV [1] and Cheng-fu Chen [2,*]

[1] Department of Mechanical Engineering, University of Alaska Fairbanks 1; jhhalfordiv@alaska.edu
[2] Department of Mechanical Engineering, University of Alaska Fairbanks 2; cchen4@alaska.edu
* Correspondence: cchen4@alaska.edu; Tel.: +1 (907) 474-7265

Abstract: The silane (3-Aminopropyl)triethoxysilane (APTES) possesses one terminal amine group and three ethoxy groups extending from each silicon atom, serving as a crucial interface adherent between organic and inorganic materials. The role of APTES as a primer in a stacked coating system is in its stability as a protection layer and interaction with the topcoat material. The role of APTES in determining the electrochemical impedance of its use with a topcoated polymer on AA2024-T3 is characterized. Combinatorial experimentation is conducted by varying the length of vapor deposition of APTES, with a post heat treatment and topcoated polystyrene (PS) optionally applied individually to a cured APTES primer. The results show that the coating system made of topcoated PS on the heat-treated APTES made by concentrated vapor deposition for 40 min, as opposed to 20 min or 60 min tested, offers the best corrosion resistance. A primed APTES surface of higher surface energy accounts for higher corrosion impedance. With the surface energy derived from the measured contact angles on the APTES-primed surfaces and the SEM images, four mechanisms are suggested to explain that a good corrosion performance of the APTES/PS coating system can be attributed to enhanced wettability achieved by the PS/acetone solution on the cured APTES primer of higher surface energy. Additionally, the results suggest that, in the early stages of exposure to the corrosion solution, a thinner APTES primer (deposited for 20 min) enhances protection against corrosion, which can be attributed to hydrolytic stability and the interactions between hydrolyzation/condensation in soaked APTES and the dissolution of naturally formed aluminum oxide pre-existing in the bare samples. An APTES primer subjected to additional heat treatment before topcoating will increase the impedance of the coating system significantly. APTES, and silanes, in general, as an adherent agent or a surface modifier have a wide range of potential applications in micro devices, as projected in Discussions.

Keywords: vapor deposition; coating; primer; polystyrene; APTES; silanes; AA2024-T3; corrosion; electrochemical impedance spectroscopy; surface energy

1. Introduction

Silanes and silane esters have demonstrated considerable promise as corrosion-resistant adhesion promoters [1], undercoats [2], or used in paint emulsions [3]. APTES, a reactive silane ester (trialkoxysilane) known for its grafting capabilities, enhances compatibility between mineral, organic, and polymers. APTES can be applied for surface functionalization as a primer or for surface modification of nanoparticles to form nanocomposites; both applications consider using APTES as a surface-priming agent for topcoating with functionalized polymers. Additional compounds, including magnetite nanoparticles for magnetic properties, silicate nanoparticles for enhanced strength, titanium dioxide nanoparticles for UV resistance, polyaniline for conductivity, and graphene/carbon nanotubes for reinforcement, further tailor nanocomposite functionalities [4]. How the APTES can be grafted for surface modification or priming is crucial to making a stable coating system.

APTES has been examined for use as a primer compound or as a compatibilizer between organic and inorganic materials [5]. As a primer or adhesion promoter, APTES has a terminal amine groups that have steric access to any bonds formed by the silanol. The spatial relationship of these functional groups facilitates pH-dependent hydrolysis and the formation of denser networks of oligomers [6].

Trialkoxysilanes hydrolyze quickly (in minutes) to form the free silanols but tend to condense much more slowly (in the order of hours). The networking stability of APTES is governed by the competition between the hydrolysis and condensation mechanisms, which can be minimized at a pH of around 6 [7]. Accessibility to water is one key in determining the performance of APTES as a primer for bonding of organic/inorganic materials. Although silane coatings often enhance adhesion, the silanes such as γ-aminopropyl silane (γ-APS), which is the hydrolyzed version of APTES, performs poorly when exposed to water and may fail in wet adhesion tests [2]. Silanes like APTES do not bond to the Cu-rich sites on the surface of aluminum alloys, which are highly susceptible to local pitting [1]. Therefore, silane coatings are typically used as a primer for additional top coatings. In this context, silane compounds are recognized for their potential as effective adhesion promoters between organic coatings and oxidized metal surfaces.

Applications of silanes can be classified based on their grafting functionality on inorganic surfaces [8,9], or their integrity with topcoating polymers for resistance to coating rupture and disbonding [10–12]. A TiO_2-APTES nanocomposite was scrutinized for its interfacial stability and failure [8]. PS emerges as a potential topcoat due to its efficient water repellency and relatively low surface energy of 31 mJ/m^2 [13]. The non-polar and chemically inert characteristics of PS, owing to its aromatic benzene ring, make it resistant to reactions with acids and bases, simplifying corrosion analysis [13]. PS in a solution form can be directly spin-coated onto the surface of metals like aluminum alloys. However, its effectiveness as a protective coating is limited by its poor adhesion to metals and susceptibility to film rupture in its dried thin film state. The dewetting of PS on monolayered APTES was addressed in [12]. Zhang recently addressed the thin film porosity and integrity issues in PS [14] by developing a densely compact polystyrene/TiO_2 nanocomposite coating. A PS layer can be applied as a topcoat over a silane [15]. This approach effectively mitigates the individual drawbacks of silane and PS coatings. The top-coated PS is a barrier, safeguarding the underlying silane primer from water attacks. Simultaneously, the silane primer fulfills a dual role as an additional protective layer for the metal substrate and an adhesive agent, indirectly binding the PS to the substrate.

However, the role the stacked silane/polymer coating plays after coating failure has not been well characterized except for some limited number of works [12,15,16]. Chen [15] applied the APTES/toluene solution to the hydroxylated AA2024-T3 surface. The sample surface had been grafted with the hydroxyl group before soaking in a diluted APTES/anhydrous toluene solution for forming siloxane bonds or hydrogen bonds with APTES; however, by soaking the primed APTES layer is thicker and less uniform than a monolayer [6,17], which will incur undesired complexity in the networked structure. An APTES primer prepared by solvent-based soaking also exhibits a physisorption behavior, which yields a less stable networked structure because the un-bonded/loosened ethoxy groups hidden in the cured APTES can migrate to the network surface and then react with water for hydrolyzation and the subsequent condensation, both of which will change the thickness of the cured APTES layer [17].

In this work, the aluminum alloy AA2024-T3 was chosen for priming with APTES and the subsequent topcoat with PS, to characterize the role of the APTES primer in the stacked coating system. AA2024-T3 has been extensively addressed in the literature regarding surface treatments [18]. This study uses the method of concentrated vapor deposition in low vacuum to prime APTES onto the naturally formed aluminum oxide layer of the AA2024-T3 substrate, to minimize the accessibility to humidity during deposition. The APTES-primed AA2024 samples, with an optionally additional heat treatment, are then topcoated with PS to form a stacked coating system, which is characterized by the electrochemical impedance spectroscopy (EIS) in the 3.5% NaCl solution. The surface energy of a coating is estimated from measured static contact angles of two working liquids on the coating. The characterization, together with SEM images of the coating, is analyzed for the causes of failures and explained by four hypothetical mechanisms suggested.

 doi:10.20944/preprints202312.1156.v1

2. Materials and Methods

2.1. Materials

Bare samples of 1 in. × 1 in. were machined from wrought AA2024-T3 sheets 5 mm thick bought from Online Metals. The cut samples underwent sonication in 97% isopropyl alcohol and then in deionized water, each lasting 5 minutes. Subsequently, the samples were air-dried, baked at 95°C for 120 minutes, and left in the oven overnight. The cleaned samples were then stored in a petri dish sealed with parafilm for later use.

A low molecular weight, narrowly dispersed PS flakes (Mn 8000, Mw 8800), was purchased from Polymer Source Inc. (product ID 8096-S). Technical grade acetone of 94% purity was purchased from Sunnyside Corp. A PS/acetone solution comprising 200 mg of the PS flakes dissolved in 2.28 mL of technical-grade acetone was prepared, resulting in a nominal PS concentration of 10%. APTES of purity ≥ 98% was purchased from Millipore Sigma and used without further purification. Milli-Q deionized water and anhydrous ethylene glycol of purity 99.8% (Sigma Aldrich) were used for surface contact angle measurements. For EIS measurements and subsequent in-cell corrosion, a fresh 3.5% NaCl solution was prepared from in-house deionized water and oven-dried non-iodized, non-fluorinated food-grade NaCl.

2.2. APTES Primed on AA2024-T3 Samples

APTES was applied to the clean AA2024-T3 samples using concentrated vapor deposition. This process employed a heated vapor deposition chamber (**Error! Reference source not found.**a) pumped by a dual-stage rotary vacuum pump with the valving system depicted in **Error! Reference source not found.**. The chamber undergoes evacuation with valves A and C closed. Once the desired vacuum is attained, valve B is closed to maintain the vacuum in the chamber. To cease pump operation, valve A alleviates backpressure on a rotary vane pump. Additionally, valve C can be optionally used to introduce a dry sparging gas for storage.

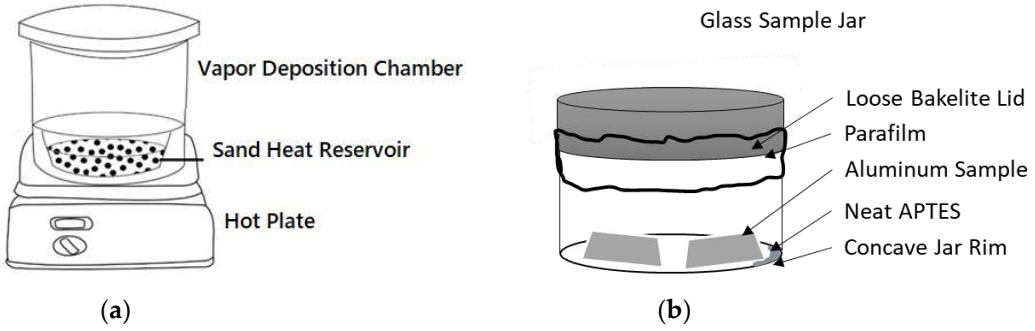

Figure 1. (**a**) Vacuum chamber used as vapor deposition chamber with a metal bowl filled with washed quartz sand. (**b**) 100 mL sample jar for vapor deposition set up for the vacuum chamber.

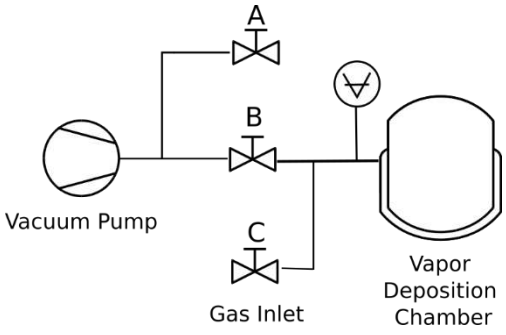

Figure 2. Schematic of vacuum system control.

 doi:10.20944/preprints202312.1156.v1

The vapor deposition chamber was bedded with industrially crushed quartz sand preheated to 150 °C under a vacuum of 10 mbar. Temperature was monitored with a thermocouple inserted into the vapor deposition chamber, while the chamber itself was heated through a hot plate set at 330 °C at the ambient condition. Afterward, a preheated and dried 100 mL glass sample jar (**Error! Reference source not found.**b), holding cleaned aluminum samples and APTES reagent, was loosely capped (parafilm was applied to the loose cap to reduce the speed of gas transfer in and out of the container). This jar was then loaded into the heated sand bath in the preheated vapor deposition chamber. While maintaining a temperature of 100 °C throughout the process, the vapor deposition chamber was restored to a vacuum under 100 mbar. Under vacuum and heated conditions, the APTES solution was gradually deposited onto the samples from the vapor phase. Three groups of samples placed inside the jar were exposed to the neat APTES within the vacuum chamber for 20, 40, or 60 minutes, respectively.

Vapor reaction times for this method of coating silanes have been characterized for durations as short as 10 minutes elsewhere [19]. After completion, the aluminum samples were covered and left undisturbed overnight in ambient conditions. One-third of the samples were reserved for contact angle analysis. The remaining samples were used for the subsequent top-coating with the PS/acetone solution.

2.3. Polystyrene Topcoated on APTES

Half of the remaining APTES-primed samples were spin-coated with 100 µL of acetone containing a 10% PS/acetone solution. The other half was prepared with further heat treatment and was allowed to incubate at an elevated temperature under a pressure of 200 mbar for an additional 24 hours to cure the APTES network further before spin-coating with the 10% PS/acetone solution.

An Ossila brand E441 Spin Coater was programmed to proceed with 1500 rpm for 5 seconds, followed by 2000 rpm for another 5 seconds, and then ended with 3000 rpm for 15 seconds. The coating solution was applied before the conclusion of the first step in the spin-coating program. After the spin-coating process, all the samples underwent 24 hours of drying.

2.4. Sample Labeling

The samples in this experiment are identified by a three-digit code: "1-Y-Z". For samples primed with APTES vapor deposition for 20, 40, or 60 minutes, the "Y" values are 20, 40, and 60, respectively. Samples are further categorized based on the presence of polystyrene by the label "Z": 0 for those only primed with APTES, 1 for those with polystyrene topcoated on the "as-is" primed APTES, and 2 for those with polystyrene topcoated on the primed APTES that had gone through further heat treatment.

2.5. Surface Characterization

The sample surfaces were characterized through contact angle measurements with a Rame-Hart goniometer using ethylene glycol and Milli-Q water. The sample lay flat on the surface of the goniometer stage, and 10µL droplets were manually dispensed out of a 100µL microsyringe onto the sample surface. The initial contact angle was recorded using DROPimage software. This measurement was replicated across the sample to determine a statistically representative sample.

Exploratory Scanning Electron Microscope (SEM) imaging was taken using a FEI Quanta200 system in the low vacuum mode. Image processing and scaling was completed using GIMP software. All scaling was completed using pixel length of the SEM Scaling bar.

2.6. Electrochemical Impedance Measurement

EIS was taken using a Gamry G300 potentiostat and the Gamry Echem Analyst 6.33 software. Measurements were taken using a conventional three-electrode setup in a horizontal flat cell. A graphite counter electrode and Ag/AgCl/saturated KCl reference electrode. The sample was mounted in a 1 cm diameter, 0.78 cm^2 area window. The EIS data was imported into the Python module

Preprints (www.preprints.org) | NOT PEER-REVIEWED | Posted: 15 December 2023 doi:10.20944/preprints202312.1156.v1

"impedance.py." The details of the data fitting are beyond the scope of this paper and will be reported separately, but a summary is given in the Supplementary Materials.

3. Results and Discussions

The EIS data of the coated samples were analyzed using a Randles circuit (**Error! Reference source not found.**), which contains one time constant featured by two parallel passive elements C_1 and R_1. Here, C_1 is a constant phase element (CPE) of the form $\frac{1}{Qs^n}$ to account for non-Faradaic charge transfer, where Q and n are the CPE parameters; the resistance R_1 represents the impedance of the Faradaic current flows. A Warburg element is connected to R_1 to account for any diffusion-limiting reactions.

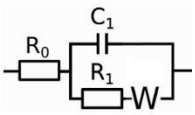

Figure 3. Equivalent circuits for analyzing EIS data: Randles model.

3.1. APTES Primer

Figure 4 compares the impedance between the bare sample and three types of samples primed with APTES vapor deposition for 20, 40, or 60 minutes. In the initial corrosion stage, roughly within the first 100 hours, the impedance of the bare sample exceeded that of all APTES-primed samples. This behavior can be attributed to the presence of aluminum oxide and its interaction with the vapor-deposited APTES primer when exposed to the aqueous electrolyte solution, as elaborated in the Discussions section. Among the three tested APTES-primed layers, the -20- and -40- samples exhibited similar and superior performance compared to the -60- sample.

In the later stage (after the 100-hr mark), the impedance of the bare sample decreased quickly and persistently, meaning its alumina protection layer was damaged by corrosion. However, all the APTES-primed samples, regardless of their type, enable a larger impedance than the bare sample in this stage. The impedance of the APTES coating per -60- was persistently increasing over time, as opposed to the -20- and -40- coating layers which began to lose their impedance in the middle of the corrosion period tested. The data points distributed in the Nyquist plots of all the APTES-primed samples exhibit one time constant, evidenced by the semicircle arc fitting to each set of the points. Some curves end up with a feature of Warburg impedance at the lower frequency regime, which signals the onset of a reaction under partial or complete mass transport control by diffusion [20].

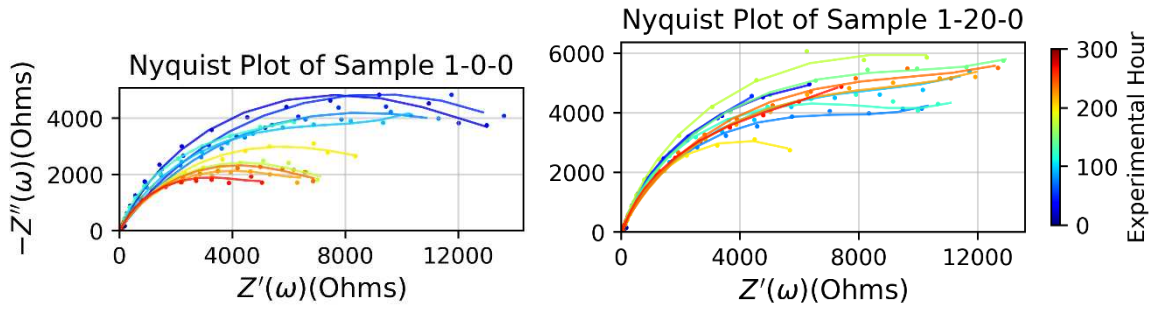

(**a**) (**b**)

Preprints (www.preprints.org) | NOT PEER-REVIEWED | Posted: 15 December 2023 doi:10.20944/preprints202312.1156.v1

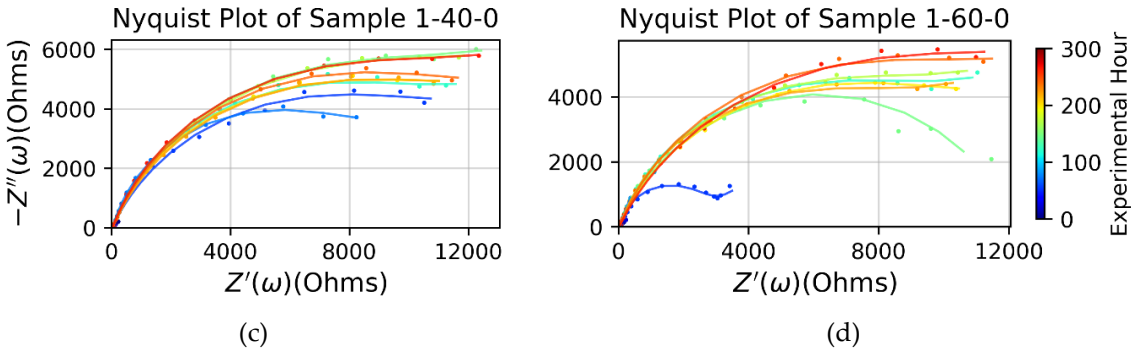

(c) (d)

Figure 4. Nyquist plot of measured impedance data (dot) and EIS-fitted trendline over the duration of testing (color-coded in legend) (**a**) Bare sample; and samples coated with a thin layer of APTES vapor-deposited for (**b**) 20 min, (**c**) 40 min, and (**d**) 60 min.

Error! Reference source not found. compares the fitted parameters of the Randles circuit model. The model shows that the resistance of the bare sample decreased monotonically over time, indicating the dissolution of the naturally formed oxide layer in the corrosion solution. For the APTES-coated samples, it shows that:

- In the first 100 hours of corrosion, the 1-20-0 APTES coated sample exhibited the largest resistance, while the 1-60-0 APTES coating had the least. The effective capacitance (as calculated by $Q\omega^n$) of the 1-20-0 sample remained relatively constant from the beginning of corrosion, as opposed to that of the 1-40-0 and 1-60-0 samples, which decreased over time. (Refer to the individual plots of Q and n in Figure S1 in the Supplementary Materials.). Together with the trendlines in the resistance and capacitance curves, it can be deduced that the change in the modes of electrons and or ions exchange involved in any chemical reactions of corrosion and dissolution of the 1-20-0 APTES layer is dictated by the change in resistance, i.e., the Faradaic process.
- After four days of exposure to the corrosion solution, the resistance in the 1-40-0 and 1-60-0 samples increased slightly, which may be because the coating remained intact while the accumulation of the corrosion products narrowed its porous pathways. The resistance of the 1-20-0 sample slightly decreased, implying that the APTES coating in the 1-20-0 sample started to degrade.
- Over the entire corrosion period, the 1-20-0 sample also had a significantly larger Warburg impedance than the other samples shown in **Error! Reference source not found.**c. It suggests that the APTES coating prepared per the -20- protocol enabled a local, interfacial environment that can effectively impede the diffusion of reactive species for charge transfer.

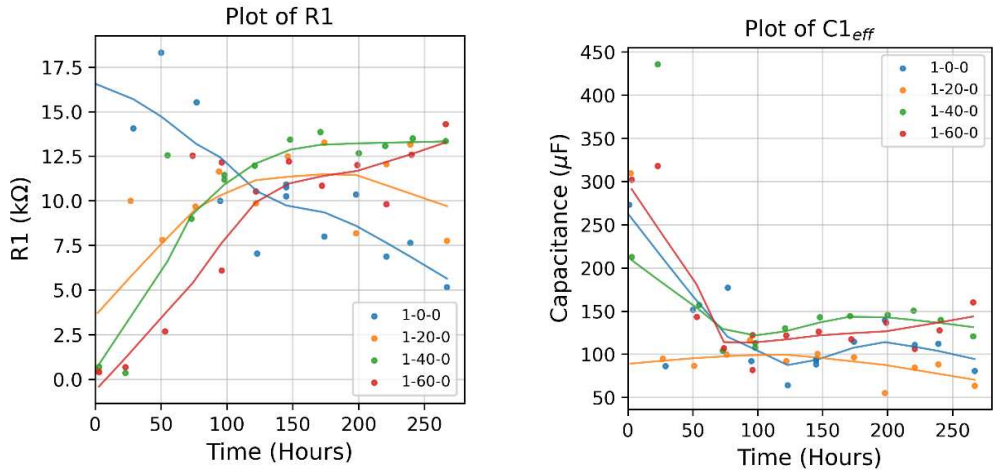

(**a**) (**b**)

Preprints (www.preprints.org) | NOT PEER-REVIEWED | Posted: 15 December 2023 doi:10.20944/preprints202312.1156.v1

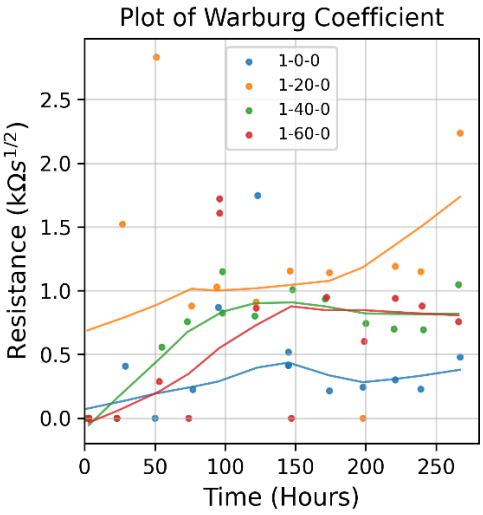

(**c**)

Figure 5. The Randles circuit model's fitted parameters (dots) and their trendline. (**a**) Coating resistance R_1. (**b**) Effective capacitance of CPE. (**c**) The Warburg impedance. Trend lines were determined by locally weighted scatterplot smoothing (LOWESS) contributed by the package statsmodel.py.

Error! Reference source not found. shows the SEM images of a cleaned bare sample and the samples primed with APTES in the three conditions protocoled herein. Noted that the SEM imaging of the samples was completed in an exploratory manner to highlight that (1) the commercially wrought surface is not flat but instead has micro texture from the milling process, whereas comparison surfaces use analytically flat samples (silica or silica oxide), and (2) the APTES primed layer was too thin to cover the manufacturing induced surface defects of the aluminum samples (e.g., **Error! Reference source not found.**d).

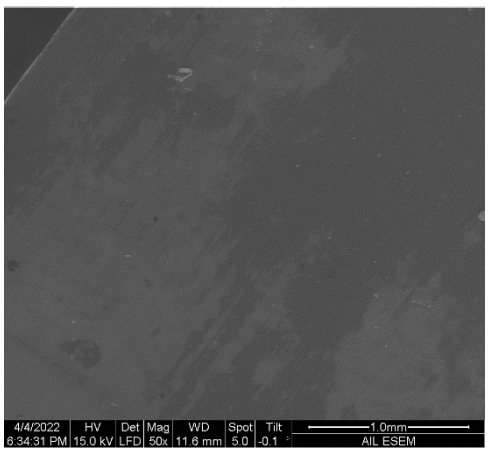

(**a**)

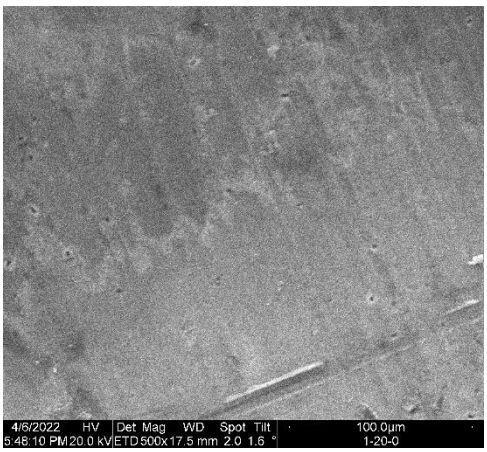

(**b**)

Preprints (www.preprints.org) | NOT PEER-REVIEWED | Posted: 15 December 2023 doi:10.20944/preprints202312.1156.v1

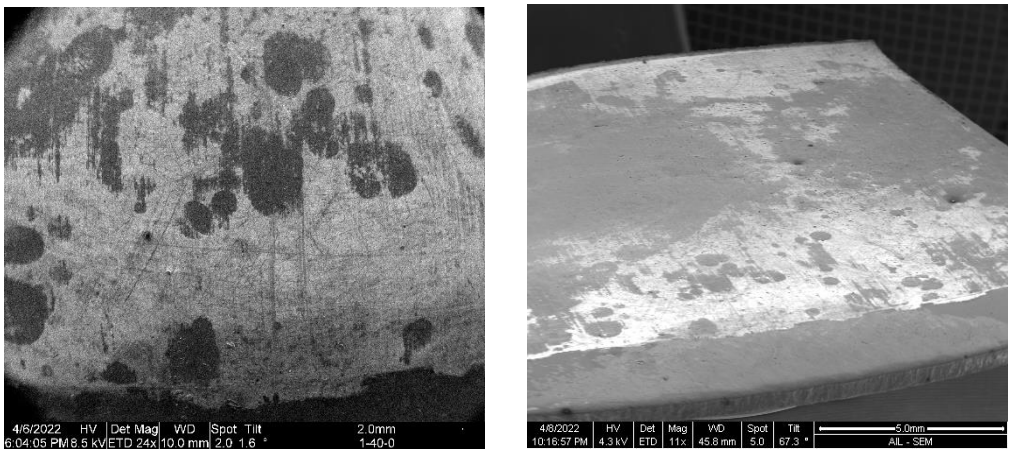

(**c**) (**d**)

Figure 6. SEM imaging of (**a**) bare sample and APTES-primed samples: (**b**) 1-20-0. (**c**) 1-40-0. (**d**) 1-60-0.

3.2. Polystyrene Topcoated on APTES

The influence of the primed APTES layer on the impedance of the PS/APTES-coated samples can be seen by comparing the evolving behavior of the impedance curves of the coated samples in **Error! Reference source not found.**.

The samples labeled by 1-Y-1 (Y is 20, 40, or 60) (**Error! Reference source not found.**a, c, e) were primed with APTES that had only been cured in the ambient condition without additional heat treatment. Although the APTES layer primed by vapor deposition for 20 min or 60 min had a more significant impedance the 1-40-1 sample, they degraded over time and thus became hydrolytically unstable, which is related to partially networked silanols [21].

In the other group of the samples (**Error! Reference source not found.**b, d, f) of label 1-Y-2 (Y is 20, 40, or 60), the APTES layer had been further heat treated before the PS layer was topcoated. This group of samples exhibited a higher impedance and better hydrolytic stability than the first group (**Error! Reference source not found.**a, c, e), which did not undergo additional heat treatment after polymerizing their APTES layer. These results suggest that post-silanization heat treatment of the APTES layer, following its curing, can enhance networking tightness and hydrolytic stability. This improvement is likely due to the removal of any residual water from a silanized structure [22] and of the solvent adsorbed to the APTES surface [4] facilitating the condensation reaction for denser silanol bonds within the networked structure. The group of the samples all showed an increasing impedance over time. For each sample in this group, the diffusion-limiting transport of reactive specimens can be evidenced by the upright tail of the impedance curves associated with the 100-hour (or earlier) legend. It indicates that over the first 100 hours, the electrolyte solution permeated the coating layer, reaching the coating/substrate interface to enable a local environment to allow the reactive species to react with the metal substrate; such species-exchange passages will become narrowed once the corrosion products are stuck at the reaction sites because their removal (likely by diffusion) is impeded by the insoluble coating, albeit the porous structure of the coating. Once the corrosion products were accumulated locally at the coating/substrate interface, the sample became less conductive, as shown by the curves of increasing impedance after the 100-hour mark. The APTES/PS coating in sample 1-40-2 performed significantly better in these samples because of its relatively higher impedance.

The samples that were primed with APTES by vapor deposition for 40 min (the 1-40-Z samples, Z is 1 or 2) held their impedance persistently with the minimum extent of degradation, as seen by the monotonically increasing trend of the impedance curves. It implies that the 40-min primed APTES layer had cured with the densest network, preventing the loss of its polymerized structure to re-hydrolyzation [23].

Preprints (www.preprints.org) | NOT PEER-REVIEWED | Posted: 15 December 2023 doi:10.20944/preprints202312.1156.v1

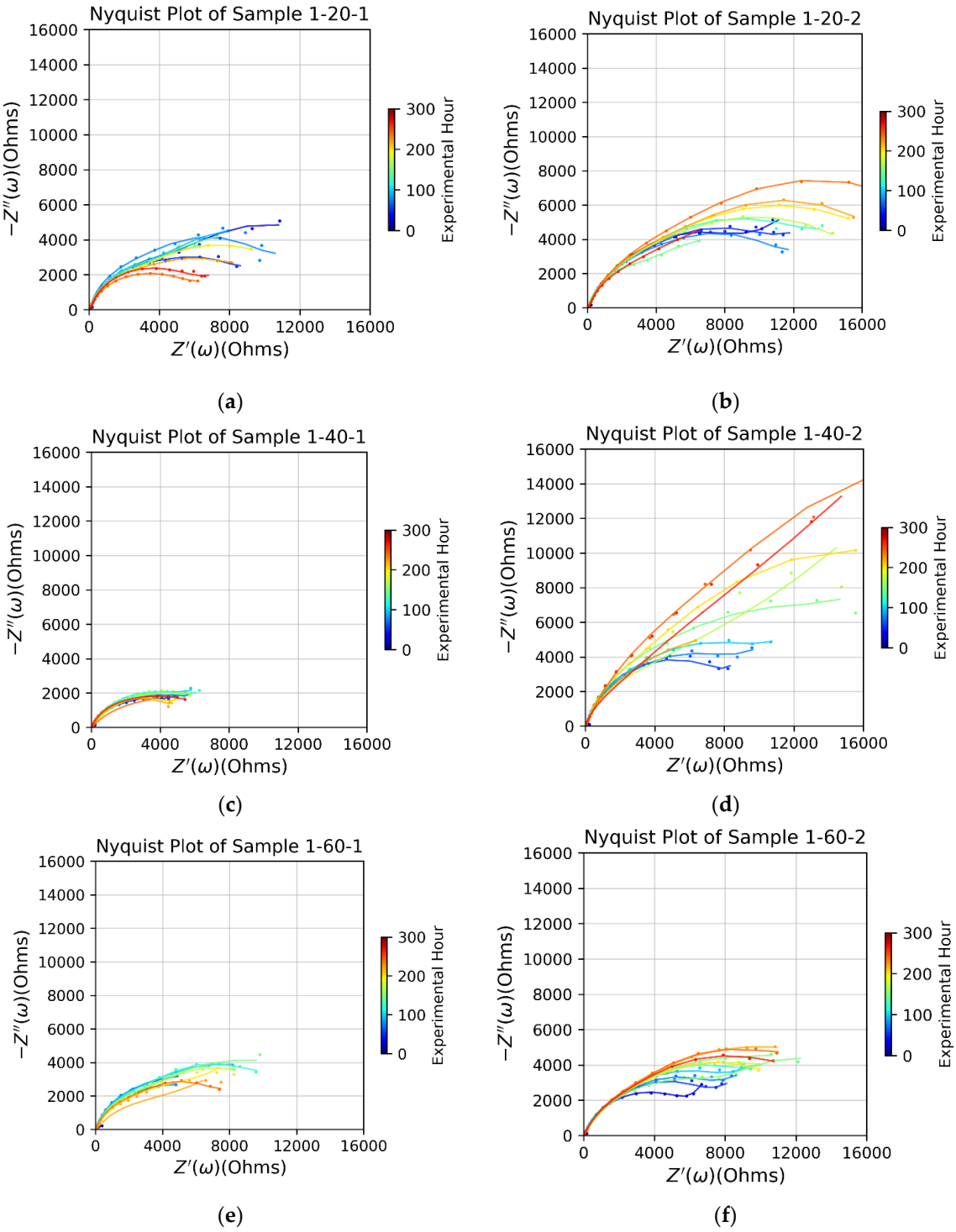

Figure 7. Impedance of PS top-coated samples with the APTES primer as cured without further treatment (**a, c, e**) and with a further heat treatment (**b, d, f**). Each APTES primer was vapor deposited for 20, 40, or 60 min as labeled by -20-, -40-, or -60-, respectively.

3.3. Surface Characterization

The dispersion and polar components of the surface energy on the cured APTES surface were calculated by applying the Fowkes model with the measured contact angles of water and ethylene glycol [26,27]. Table 1 lists the properties of water and ethylene glycol for the calculations. The properties of acetone are also listed for determining the wettability of the PS/acetone solution on a sample surface.

Preprints (www.preprints.org) | NOT PEER-REVIEWED | Posted: 15 December 2023 doi:10.20944/preprints202312.1156.v1

Table 2 lists the measured static contact angles and the calculated surface energy. Despite the preference for dynamic contact angle measurements for a comprehensive wettability analysis, the static contact angle measurements were taken due to equipment limitations. The statistics were developed through multiple tests on fresh areas of the same sample. All statistics were derived from a sample space of more than 10 measurements. The wide statistical variations are due to the non-homogeneous, non-uniform nature of the wrought aluminum sample surface. Acknowledging that achieving analytical precision in contact angle measurements for coating wettability necessitates perfectly flat surfaces is crucial. However, the wrought aluminum sheets do not have these characteristics.

Table 1. Polar and dispersion parts of the surface energy of the working liquid agents used.

Solvent	Mol. Formula	CAS #	Surface energy / tension (mJ/m²)			Reference
			γ_l	Dispersion γ^D	Polar γ^p	
DI Water	H_2O	7732-18-5	72.8	26.85	45.9	[24]
Ethylene glycol	$C_2H_6O_2$	107-21-1	48.0	29.0	19.0	[24]
Acetone	$(CH_3)_2CO$	62-53-3	24.5	--	--	[25]

Table 2. Measured contact angles and calculated surface energy components.

Sample (1-Y-Z)	Contact Angle (°)		APTES		PS	Surface Energy (mJ/m²)		
	DI Water	Ethylene Glycol	Vapor Deposition Time (min)	Additional heat treatment	Topcoated	Dispersion γ_s^D	Polar γ_s^p	Total $\gamma_s^p + \gamma_s^D$
1-0-0	82 ± 21	65 ± 12	--	--	--	13.3	11.1	24.4
1-20-0	63 ± 11	47 ± 14	20	NO	NO	9.6	29.6	39.2
1-40-0	63 ± 10	34 ± 8	40	NO	NO	23.1	17.0	40.2
1-60-0	60 ± 12	22 ± 16	60	NO	NO	29.6	15.2	44.7
1-20-0*	47	56	20	YES	NO	43.3	15.9	59.2
1-40-0*	48	57	40	YES	NO	46.6	13.9	60.5
1-60-0*	53	62	60	YES	NO	50.7	10.1	60.8
1-20-1	81 ± 14	66 ± 12	20	NO	YES	10.7	13.8	24.4
1-40-1	83 ± 6	56 ± 5	40	NO	YES	29.6	3.5	33.1
1-60-1	83 ± 6	59 ± 15	60	NO	YES	24.3	5.1	29.4
1-20-2	90 ± 7	57 ± 5	20	YES	YES	44.4	0.1	44.5
1-40-2	94 ± 8	58 ± 7	40	YES	YES	53.1	0.3	53.4
1-60-2	93 ± 8	60 ± 1	60	YES	YES	45.4	0.0	45.4

* Interpolated data.

The surface energy of the APTES-primed surface that had undergone additional heat treatment was interpolated and listed in Table 2. Assuming surface energy conservation as a linear combination of the weighted energies of constituent parts and considering PS characteristics as independent of the coated surface, the heat-treated APTES without PS can be described as having energy similar to 1-20-Z samples plus the difference between the 1-Y-1 and 1-Y-2 samples.

The results in Table 2 show that:

- The measured contact angles of DI water on the cured APTES surface and dried PS surfaces are statistically indistinguishable. However, the contact angle of ethylene glycol on a cured APTES surface decreases with the increased vapor deposition time of coating APTES.
- On an APTES primed surface: the dispersion energy is increased over an increasing length of vapor deposition of an APTES layer. All the APTES-primed samples except for the 1-20-0 were characterized by the surface energy of a larger dispersion component than the polar component.
- On a topcoated PS surface: the total surface energy calculated for the 1-Y-2 samples (in which the surface of the cured APTES layer had undergone additional heat treatment before topcoating with PS) is 50 % or higher than that of the 1-Y-1 samples (in which the cured APTES layer had

 doi:10.20944/preprints202312.1156.v1

no additional heat treatment). Both groups of the samples have much smaller dispersion energy. The polar component of the surface energy is relatively smaller than the dispersion component, except for the 1-20-1 sample surface. Noted that, among the PS-coated samples, the samples 1-40-2 had the largest surface energy.

SEM images of the APTES-primed samples top-coated with PS in **Error! Reference source not found.** show the coating heterogeneity with various dewetted patterns formed on every PS top-coated sample. Consistent patterns in PS dewetting were problematic to discern because of the high coating heterogeneity. Cracks in the coating surface can be observed in all types of PS coated samples. The crazing is consistent with low weight PS, which does not have the tensile strength of polymers above the molecular entanglement weight. Small PS dewetted patterns such as "microdots" of approximately 2-3 μm can be observed on all the samples (also shown in Supplementary Materials, Figure S2). The dewetted patterns in 1-Y-2 samples constitute a less dense distribution of small patterns and larger packs with crazing.

The topcoated PS layer covered the underneath APTES-primed layer (see Supplementary Materials, Figure S3). However, the topcoating was not uniform, as the dried PS were dewetted into various shapes, whereby crazing is apparent in some large patterns. The 1-40-2 sample had the relatively uniform topcoating as seen in **Error! Reference source not found.**d.

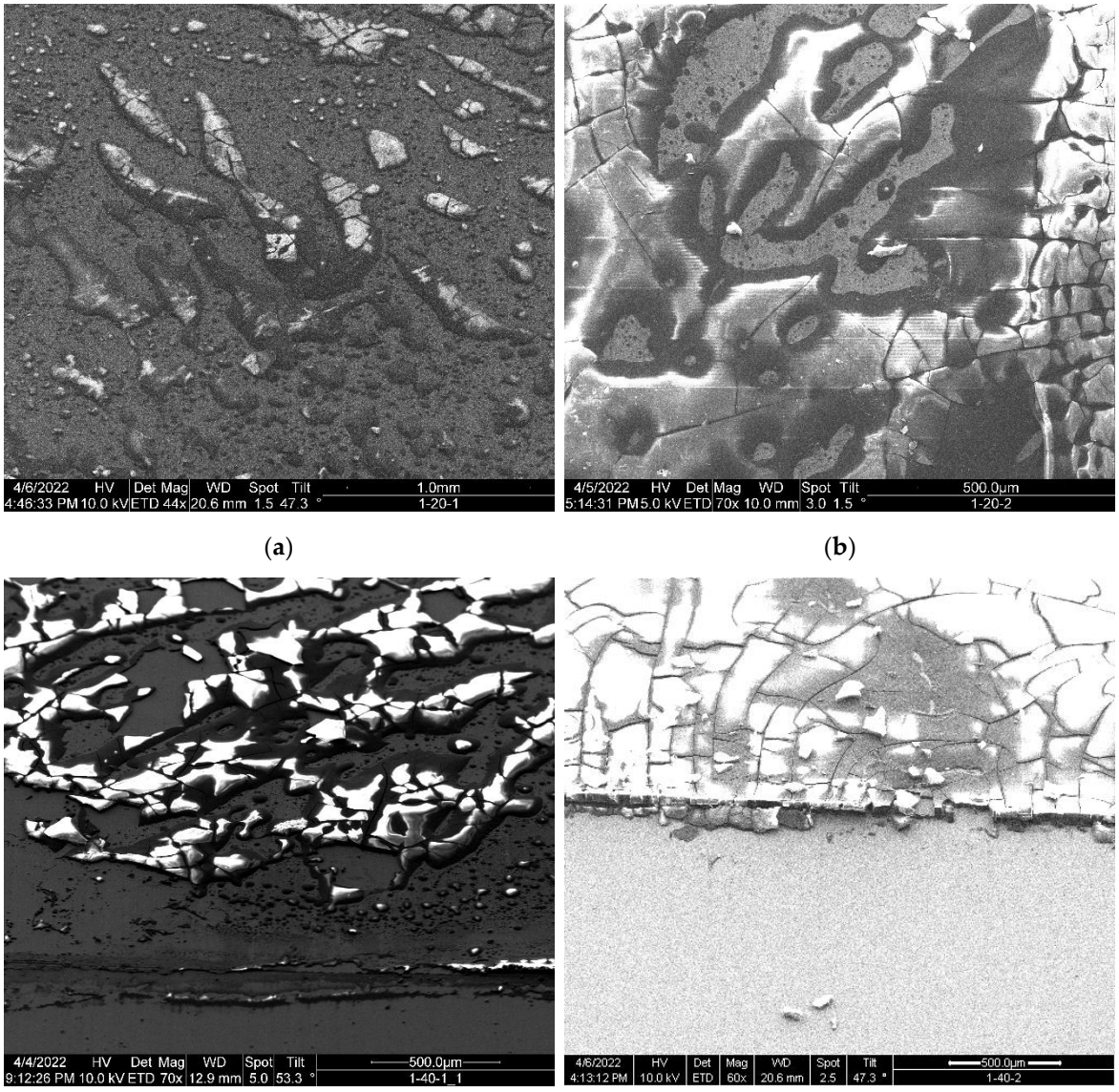

(**a**) (**b**)

(**c**) (**d**)

Preprints (www.preprints.org) | NOT PEER-REVIEWED | Posted: 15 December 2023 doi:10.20944/preprints202312.1156.v1

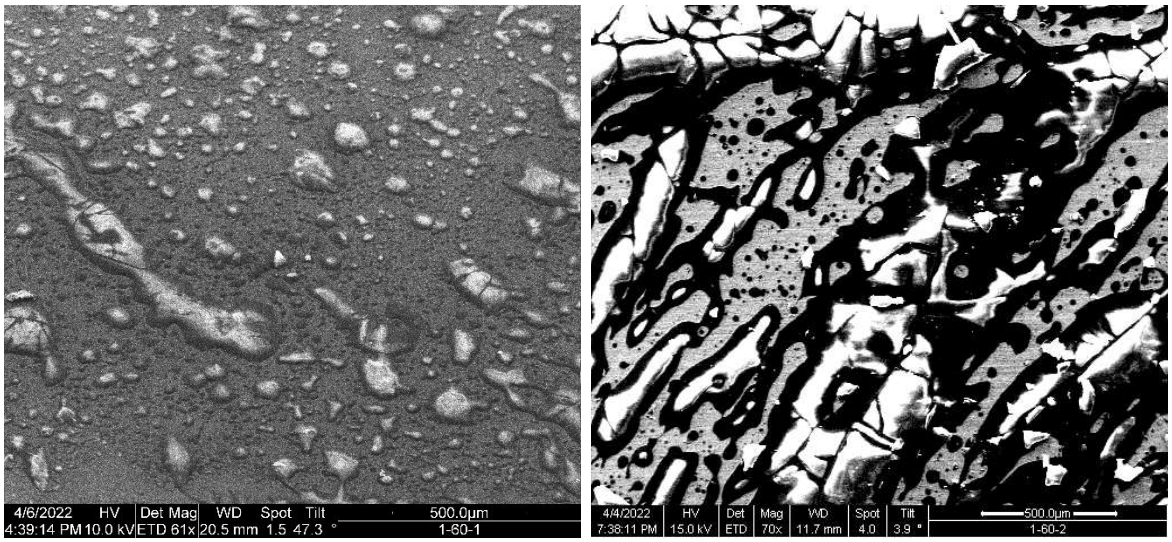

(**e**) (**f**)

Figure 8. SEM images of dewetted PS patterns on APTES for sample: (**a**) 1-20-1, (**b**) 1-20-2, (**c**) 1-40-1, (**d**) 1-40-2, (**e**) 1-60-1, (**f**) 1-60-2.

4. Discussions

In the context of the various failure scenarios, the naturally formed aluminum oxide, silane primer, and PS top-coating interact with one another in the coating system. The interactions may minimize ion exchange during corrosion and introduce undesired local environments, potentially compromising the individual effectiveness of each material as a corrosion barrier. A few mechanisms derived from the experimental results are discussed below for their interactions in the related failure modes. Note that these mechanisms may need further adjustments before they are applied to explain the roles of APTES prepared by different approaches than the concentrated vapor deposition method used herein [4,28].

4.1. The Role of APTES in Interaction with the Aluminum Oxide Substrate

APTES was applied to AA2024-T3 through concentrated vapor-phase deposition in a heated, high vacuum environment with negligible humidity. Hydrolyzation and condensation of the ethoxy groups are impeded in the absence of water, resulting in a networked APTES primer that will primarily rely on hydrogen bonds. As a result, the cured APTES primer in the samples is expected to have a structure with a lower density of covalent silanol bonds. However, a more desirable APTES network would feature a higher density of these bonds for better hydrolytic stability as a barrier layer. It can thus elucidate that during the initial stage (the first 100 hours of soaking in the corrosion solution), the naturally formed aluminum oxide layer would serve as the primary barrier for corrosion protection of AA2024-T3, because the primed APTES layer is less hydrolytically stable. keep this in mind, three mechanisms related to the reaction of APTES and its interaction with the aluminum oxide substrate are developed.

1. Mechanism 1. APTES under water adsorption and permeation

Water access becomes possible when the primed samples are later exposed to ambient humidity or immersed in aqueous electrolytes. It leads to absorption of water molecules to the APTES surface, gradually permeating into the networked APTES layer. It will then promote hydrolysis and condensation reactions. These water-induced reactions form the desired silanol bonds that can contribute to an improved structural integrity of the APTES layer. However, permeation of water through the APTES network is slow.

2. Mechanism 2. APTES reacts with aluminum oxide

 doi:10.20944/preprints202312.1156.v1

Secondly, APTES also reacts with the aluminum oxide exclusively by forming stable siloxy bonds (M-O-Si) [29]]. This reaction helps reduce the density of unbonded voids or hydrogen bonds susceptible to water attack.

3. Mechanism 3. Loss of the naturally formed aluminum oxide to APTES hydrolyzation

However, the APTES-primed layer also facilitates the dissolution of the naturally formed aluminum oxide. The hydrolyzation of the amino groups in APTES makes the solution locally alkaline [30] and aluminum oxide solubility changes in alkaline solutions [31].

The three mechanisms compete with one another to collectively determine the overall anti-corrosion performance of the APTES-primed AA2024-T3 samples, which were under the stacked barrier of the natural Al_2O_3 layer and the APTES-primed layer. Why the 1-20-0 APTES coated sample exhibited the Highest resistance (Figure 4b, c, d) can be attributed to:

- The reduced extent of alkaline conditions resulting from hydrolyzation in the 1-20-0 sample's APTES layer contributed to the increased stability of the aluminum oxide layer.
- The hydrostatic stability of APTES [4] — the APTES primer on the 1-20-0 sample demonstrated relatively robust hydrolytic stability, as indicated by the consistent evolving behavior of the effective capacitance in Figure 5b. Consequently, the structural integrity of the APTES primer on the 1-20-0 sample remained the most pronounced, resulting in the minimal release of OH^- ions and making the local solution less alkaline.

This behavior can also clarify why the 1-60-0 APTES coating had the smallest impedance during the initial 100 hours of corrosion. The hydrolyzation in the 1-60-0 APTES layer fostered a more potent alkaline environment, leading to increased dissolution of aluminum oxide. Meanwhile, as an APTES layer produced by concentrated vapor deposition is typically only tens of angstroms thick [6] and becomes even thinner after hydrolysis [32], furthermore, the role of thickness in the APTES layer of the three samples (-20-, -40-, and -60-) in providing barrier protection becomes less significant compared to the naturally formed aluminum oxide layer.

4.2. The Role of APTES in Interaction with the Topcoating

The extent and uniformity of PS coverage plays a crucial role in determining impedance. A PS/acetone solution was applied as a topcoat over the primer, a cured APTES layer in this study. The following mechanism is suggested to explain the effect of the surface energy of a primed APTES in the extent of PS-coated coverage and its relation to the impedance of a sample with the naturally formed aluminum oxide, APTES primer, and PS topcoat.

4. Mechanism 4. The surface energy of primed APTES Vs. the surface tension of the PS solution.

The PS/acetone solution partially wet the APTES surface – once the PS layer was dried after the acetone evaporated, various dewetted patterns of dried PS formed, as shown in **Error! Reference source not found.** (and Figures S2 and S3 in the Supplementary Materials). The extent of wettability of an APTES-primed surface by the PS/acetone solution is determined by the competition between the surface tension of acetone and the surface energy of the cured APTES. Because the PS/acetone solution has a lower surface tension than the surface energy of the cured APTES (refer to Tables 1 and 2), the PS/acetone solution can wet the APTES-primed surface regardless of the duration of the vapor deposition taken. The higher the surface energy of the APTES primer surface, the more wetted by the PS/acetone solution. Both observed trends can be related to that a substrate with higher surface energy tends to be more wetted by a liquid with lower surface tension. Enhanced wetting results in fewer dewetting artifacts or patterns. This relationship is illustrated by Ashley et al. [33], who demonstrated that the number density of dewetted polystyrene patterns is proportionate to the surface energy of the cured APTES on which the PS was deposited. The textural roughness and heterogeneity of the wrought sample surface also facilitates wettability. Because the surface tension of the PS/acetone solution is smaller than the surface energy of the primed APES surface, a higher surface energy of the primed APTES promotes a larger extent of wetting by the PS/acetone solution.

With Mechanism 4, it can be surmised that the APTES primer of a higher surface energy (which can be incurred with additional heat treatment) can be more wetted by the PS/acetone solution. The dried PS layer from such an APTES surface of higher energy will form larger patterns [33]; however, given the chosen PS of low molecular weight that has less tension, the dried PS layer can be easily

 doi:10.20944/preprints202312.1156.v1

cracked. This can explain why the 1-Y-2 samples exhibited the dewetted patterns of larger packs with crazing.

4.3. Potential Applications to Micro Devices

The vapor-phase deposition of silanes is implementable in the photo-lithography based micro fabrication process [34]. Given the availability of surface modification with silanes on micro devices, the technique characterized in this paper can find a broad range of applications in micro-fabricated devices that requires bonding/adhesion of dissimilar materials [35] for hermetic sealing, chemical sensing, or modifying the mechanical characteristics of micro structures. A few sensible applications are enumerated here. First, a conformal polymeric topcoat on a micro device can address the intrinsic stress-induced warpage. The intrinsic stress is thermally induced, as caused by selective removal (etching) of dissimilar materials from each thin film individually deposited in a different temperature on a silicon wafer during fabrication. The intrinsic stress distorts the patterned feature from their designed dimensions, and can warp micro cantilevered structures [36]. Kuchiji et al. addressed the warpage issue with a polyurethane coating [37]. Polyurethane is more widely used than polystyrene. Cured polyurethane has a relatively strong elasticity modulus, so a thin coating will suffice to counter-act with the intrinsic stress to mitigate warpage in micro devices. The durability of the polyurethane coating on vibratory micro structures is crucial, which may be addressed by the APTES-modified polyurethane [38]. A low dose (e.g., 1 %) of concentrated APTES can be directly mixed with waterborne polyurethane; or APTES can be the primer for topcoating with 2K polyurethane solutions. Second, an APTES-modified surface exhibits a hydrophobic behavior (Table 2). This feature can be used to make a microsensor chip water/moisture repellent [39]. Third, For micro sensors that require a biocompatible or hermetic seal for chronic implantation, conformal coating of polymers of low Young's modulus can sustain the designed sensing capability [37,40]. To address the adhesion strength and durability of the added coating for a long-term deployment, silanes like APTES can be used as a primer for topcoating with Parylene for applications in vivo [41], or mixed with polyurethane as a hybrid composite for ex-vivo applications [42]. As opposed to the use of strong polyurethane in modifying the mechanical behavior of a micro device, the polymers of low elasticity modulus like Parylene C can be coated on an APTES-primed surface for encapsulation, and/or be further patterned without changing the designed mechanical impedance of micro devices [37,40,43]. Polyimide (Kapton), another candidate polymer of low elastic strength, is commonly used in the poly(dimethylsiloxane)-based soft lithography with APTES as the bonding agent [44,45]. These applications are all based on the use of silanes, whereby a focus was placed on APTES as an adherent agent for bonding or as a surface modifier for topcoating with a polymer of choice for various purposes.

5. Conclusions

The complexity in the arrangement of and interactions among the three layers of the naturally formed aluminum oxide, primed silane, and top-coated PS film make the stacked coating system challenging to manage for predictable anti-corrosion performance.

This paper addressed this challenge by examining the role of the silane primer, APTES, commonly used as an adherent agent for inorganic/organic bonding. With the primed layer made by concentrated vapor deposition, the findings indicate that an APTES primer of an optimal thickness (as associated with the 1-40-2 sample) offers the best corrosion resistance. This result is attributed to the relatively large surface energy in this primed APTES surface that enables better wettability by the PS solution and, consequently, more uniform coverage of the dried PS topcoat. During the early exposure to the corrosion solution, a thinner APTES primer would enhance protection against corrosion. It can be explained by the mechanisms of hydrolytic stability and the interaction between the hydrolyzation/condensation in soaked APTES and the dissolution of the naturally formed aluminum oxide pre-existing in the bare samples. An APTES primer under additional heat treatment before topcoating always performs better. Finally, the applications of APTES and silanes in micro devices are projected.

Supplementary Materials: The following supporting information can be downloaded at: www.mdpi.com/xxx/s1, 1. Summary of Data Fitting with Python Module "impedance.py". Figure S1: Fitted CPE parameters.

Author Contributions: Conceptualization, J.H. and C.C.; methodology, J.H. and C.C.; software, J.H.; validation, J.H. and C.C.; formal analysis, J.H.; investigation, J.H. and C.C.; resources, J.H. and C.C.; data curation, J.H. and C.C.; writing—original draft preparation, J.H. and C.C.; writing—review and editing, J.H. and C.C.; visualization, J.H. and C.C.; supervision, C.C.; project administration, C.C.; funding acquisition, C.C. Both authors have read and agreed to the published version of the manuscript.".

Funding: This research was supported by the NASA EPSCoR Program Cooperative Agreement Notice (CAN) (80NSSC20M0137).

Data Availability Statement: Raw EIS data can be found at https://sites.google.com/a/alaska.edu/cf-chen/home/organic-inorganic-coating.

Acknowledgments: The SEM imaging was performed at the Advanced Instrumentation Laboratory (AIL), University of Alaska Fairbanks.

Conflicts of Interest: The author declares no conflict of interest.

References

1. Hintze, P.E.; Calle, L.M. Electrochemical properties and corrosion protection of organosilane self-assembled monolayers on aluminum 2024-T3. *Electrochim Acta*. 2006, 51(8–9), pp. 1761–6.
2. Lyon, S.B.; Bingham, R.; et al. Advances in corrosion protection by organic coatings: What we know and what we would like to know. *Prog Org Coat*. 2017, *102*, pp. 2–7.
3. Bera, S.; Rout, T.K.; et al. Comparative Study of Corrosion Protection of Sol–Gel Coatings with Different Organic Functionality on Al-2024 substrate. *Prog Org Coat*. 2015, *88*, pp. 293–303.
4. Sypabekova, M.; Hagemann, A.; et al. Review: 3-Aminopropyltriethoxysilane (APTES) Deposition Methods on Oxide Surfaces in Solution and Vapor Phases for Biosensing Applications. *Biosensors 2023, Vol 13, Page 36*. 2022, 13(1), pp. 36.
5. Plueddemann, E.P. Silane Coupling Agents. New York: Springer US; 1991. 253 p.
6. Zhu, M.; Lerum, M.Z.; et al. How to prepare reproducible, homogeneous, and hydrolytically stable aminosilane-derived layers on silica. *Langmuir*. 2012, 28(1), pp. 416–23.
7. Brochier Salon, M.C.; Belgacem, M.N. Competition between hydrolysis and condensation reactions of trialkoxysilanes, as a function of the amount of water and the nature of the organic group. *Colloids Surf A Physicochem Eng Asp*. 2010, 366(1–3), pp. 147–54.
8. Meroni, D.; Lo Presti, L.; et al. A close look at the structure of the TiO2-APTES interface in hybrid nanomaterials and its degradation pathway: An experimental and theoretical study. *Journal of Physical Chemistry C*. 2017, 121(1), pp. 430–40.
9. Simon, A.; Cohen-Bouhacina, T.; et al. Study of Two Grafting Methods for Obtaining a 3-Aminopropyltriethoxysilane Monolayer on Silica Surface. *J Colloid Interface Sci*. 2002, 251(2), pp. 278–83.
10. Witucki, G.L. A Silane Primer: Chemistry and Applications of AIkoxy Silanes. *Journal of Coatings Technology*. 1993, 65(822), pp. 57–60.
11. Mahdavian, M.; Ramezanzadeh, B.; et al. Enhancement of silane coating protective performance by using a polydimethylsiloxane additive. *Journal of Industrial and Engineering Chemistry*. 2017, *55*, pp. 244–52.
12. Choi, S.H.; Newby, B.M.Z. Stability enhancement of polystyrene thin films on aminopropyltriethoxysilane ultrathin layer modified surfaces. In: Mittal KL, editor. Silanes and Other Coupling Agents. CRC Press; 2020. p. 189–208.
13. Románszki, L.; Datsenko, I.; et al. Polystyrene films as barrier layers for corrosion protection of copper and copper alloys. *Bioelectrochemistry*. 2014, *97*, pp. 7–14.
14. Zhang, J.; Zhang, L. Polystyrene/TiO2 Nanocomposite Coatings to Inhibit Corrosion of Aluminum Alloy 2024-T3. *ACS Appl Nano Mater*. 2019, 2(10), pp. 6368–77.
15. Chen, C.F. Polystyrene Coating on APTES-Primed Hydroxylated AA2024-T3: Characterization and Failure Mechanism of Corrosion. *Solids 2023, Vol 4, Pages 254-267*. 2023, 4(3), pp. 254–67.

16. Choi, S.H. Dewetting of polystyrene thin films on organosilane modified surfaces. University of Akron; 2006.
17. Kim, J. Pike Technologies. 2009. Investigation of the Formation and Structure of APTES Films on Silicon Substrates.
18. Chidambaram, D.; Halada, G.P. Infrared microspectroscopic studies on the pitting of AA2024-T3 induced by acetone degreasing. *Surface and Interface Analysis*. 2001, 31(11), pp. 1056–9.
19. Yadav, R.; Tirumali, M.; et al. Polymer composite for antistatic application in aerospace. *Defence Technology*. 2020, 16(1), pp. 107–18.
20. Taylor, S.R.; Gileadi, E. Physical Interpretation of the Warburg Impedance. *Corrosion*. 1995, 51(9), pp. 664–71.
21. Etienne, M.; Walcarius, A. Analytical investigation of the chemical reactivity and stability of aminopropyl-grafted silica in aqueous medium. *Talanta*. 2003, 59(6), pp. 1173–88.
22. Qiao, B.; Wang, T.J.; et al. High density silanization of nano-silica particles using γ-aminopropyltriethoxysilane (APTES). *Appl Surf Sci*. 2015, *351*, pp. 646–54.
23. Smith, E.; Chen, W. How to prevent the loss of surface functionality derived from aminosilanes. *Langmuir*. 2008, 24(21), pp. 12405–9.
24. Zdziennicka, A.; Krawczyk, J.; et al. Components and parameters of liquids and some polymers surface tension at different temperature. *Colloids Surf A Physicochem Eng Asp*. 2017, *529*, pp. 864–75.
25. Wu, N.; Li, X.; et al. Effect of Hydrogen Bonding on the Surface Tension Properties of Binary Mixture (Acetone-Water) by Raman Spectroscopy. *Applied Sciences 2019, Vol 9, Page 1235*. 2019, 9(6), pp. 1235.
26. Rudawska, A. Assessment of surface preparation for the bonding/adhesive technology. *Surface Treatment in Bonding Technology*. 2019, pp. 227–75.
27. Fowkes, F.M. Attractive forces at interfaces. *Ind Eng Chem*. 2002, 56(12), pp. 40–52.
28. Jothi Prakash, C.G.; Prasanth, R. Approaches to design a surface with tunable wettability: a review on surface properties. *J Mater Sci*. 2021, 56(1), pp. 108–35.
29. Rozyyev, V.; Murphy, J.G.; et al. Vapor-phase grafting of a model aminosilane compound to Al2O3, ZnO, and TiO2 surfaces prepared by atomic layer deposition. *Appl Surf Sci*. 2021, *562*, pp. 149996.
30. Jing, M.; Zhang, L.; et al. Markedly improved hydrophobicity of cellulose film via a simple one-step aminosilane-assisted ball milling. *Carbohydr Polym*. 2022, *275*, pp. 118701.
31. Zhang, J.; Klasky, M.; et al. The aluminum chemistry and corrosion in alkaline solutions. *Journal of Nuclear Materials*. 2009, 384(2), pp. 175–89.
32. Kim, J.; Seidler, P.; et al. Investigations of the effect of curing conditions on the structure and stability of amino-functionalized organic films on silicon substrates by Fourier transform infrared spectroscopy, ellipsometry, and fluorescence microscopy. *Surf Sci*. 2008, 602(21), pp. 3323–30.
33. Ashley, K.; Sehgal, A.; et al. Combinatorial Mapping of Polymer Film Wettability on Gradient Energy Surfaces. *Mat Res Soc Symp Proc*. 2001, 700(47), pp. S4.7.
34. Popat, K.C.; Johnson, R.W.; et al. Characterization of vapor deposited thin silane films on silicon substrates for biomedical microdevices. *Surf Coat Technol*. 2002, 154(2–3), pp. 253–61.
35. Kim, J.B.; Meng, E. Review of polymer MEMS micromachining. *J Micromech Microeng*. 2016, *26*, pp. 013001.
36. Reu, P.L.; Chen, C.F.; et al. Electron projection lithography mask format layer stress measurement and simulation of pattern transfer distortion. *Journal of Vacuum Science & Technology B: Microelectronics and Nanometer Structures Processing, Measurement, and Phenomena*. 2002, 20(6), pp. 3053–7.
37. Kuchiji, H.; Masumoto, N.; et al. Piezoelectric MEMS wideband acoustic sensor coated by organic film. *Jpn J Appl Phys*. 2023, 62(SG), pp. SG1021.
38. Karna, N.; Joshi, G.M.; et al. Structure-property relationship of silane-modified polyurethane: A review. *Prog Org Coat*. 2023, *176*, pp. 107377.

39. Baselt, D.R.; Fruhberger, B.; et al. Design and performance of a microcantilever-based hydrogen sensor. *Sens Actuators B Chem*. 2003, 88(2), pp. 120–31.
40. You, Z.W.; Wei, L.; et al. Design of a novel MEMS implantable blood pressure sensor and stress distribution of parylene-based coatings. *Proceedings of 2022 IEEE 16th International Conference on Solid-State and Integrated Circuit Technology, ICSICT 2022*. 2022, .
41. Sasaki, H.; Onoe, H.; et al. Parylene-coating in PDMS microfluidic channels prevents the absorption of fluorescent dyes. *Sens Actuators B Chem*. 2010, 150(1), pp. 478–82.
42. Sardon, H.; Irusta, L.; et al. Waterborne hybrid polyurethane coatings functionalized with (3-aminopropyl)triethoxysilane: Adhesion properties. *Prog Org Coat*. 2013, 76(9), pp. 1230–5.
43. Scholten, K.; Meng, E. Materials for microfabricated implantable devices: a review. *Lab Chip*. 2015, 15(22), pp. 4256–72.
44. Tang, L.; Lee, N.Y. A facile route for irreversible bonding of plastic-PDMS hybrid microdevices at room temperature. *Lab Chip*. 2010, 10(10), pp. 1274–80.
45. Borók, A.; Laboda, K.; et al. PDMS Bonding Technologies for Microfluidic Applications: A Review. *Biosensors 2021, Vol 11, Page 292*. 2021, 11(8), pp. 292.